Low-excited f-, g- and h-states in Au, Ag and Cu observed by Fourier-transform infrared spectroscopy in the 10007500 cm1 region

S Civiš, I Matulková, J Cihelka, P Kubelík, K Kawaguchi, V E Chernov

Low-excited f, g and h-states in Au, Ag and Cu observed by FTIR spectroscopy in 1000–7500 cm^{-1} region

S Civiš[1], I Matulková[1], J Cihelka[1], P Kubelík[1], K Kawaguchi[2] and V E Chernov[3]

[1] J. Heyrovský Institute of Physical Chemistry, Academy of Sciences of the Czech Republic, Dolejškova 3, 18223 Prague 8, Czech Republic

E-mail: civis@jh-inst.cas.cz

[2] Faculty of Science, Okayama University, Tsushima-naka, Okayama 700-8530, Japan

[3] Voronezh State University, 394693 Voronezh, Russia

Abstract. The infrared emission spectra of Au, Ag and Cu resulting from the laser ablation of metal targets in a vacuum was recorded using time-resolved Fourier-transform spectroscopy in the 1200–1600, 1900–3600, 4100–5000 and 5200–7500 cm^{-1} ranges with a resolution of 0.017 cm^{-1}. The majority of the observed lines correspond to transitions between low-excited Rydberg $(Nd^{10})nl_j$ states of Cu ($N = 3$), Ag ($N = 4$) and Au ($N = 5$) with a principal quantum number $n = 4..10$; the most prominent lines being due to transitions between the states with high orbital momenta $l = 3..5$. This study reports 32 new lines of Au, 12 of Ag and 20 of Cu (with uncertainties of 0.0003–0.03 cm^{-1}). From the lines observed here and in our previous works we extract revised energy values for 85 energy levels (uncertainty 0.01–0.03 cm^{-1}) of which 8 levels of Au, 3 of 23 Ag and 4 of Cu are reported for the first time. These newly-reported levels have high orbital momentum $l = 3, 4, 5$.

PACS numbers: 52.38.Mf, 07.57.Ty, 32.30.Bv, 31.15.B-

Submitted to: *J. Phys. B: At. Mol. Phys.*

Keywords:Time-resolved Fourier transform infrared spectroscopy, atomic ablation, Rydberg states, dipole transition matrix elements

1. Introduction

The atomic states with high angular momentum are of interest for various problems of atomic physics. Since Fano's formulation of the fundamental principles of large angular momentum transfer in electron–atom scattering (Fano, 1974), the high-l states have been shown to play an important role in understanding the correlation effects in processes such as the excitation and decay of autoionizing states (Napier et al., 2008; Themelis, 2010). Atomic Rydberg states with a high orbital momentum are non-penetrating states, *i.e.* the Rydberg electron in such states moves far away from the atomic core. Therefore these high-l states have very small quantum defects determined by long-range interaction with the atomic core (Lundeen, 2005). These interactions are described by simple analytical expressions that allow to extract the characteristics of the atomic core ion as polarizabilities, multipole momenta from precise microwave (Hanni et al., 2008) or optical (Keele et al., 2010) measurements of high-l states (for the use of high-l spectroscopy for the measurement of some relativistic interaction constants see (Lundeen, 2005)). Note that the theoretical calculations of these values depends crucially on very precise atomic wavefunction behavior in the vicinity of the nucleus, and therefore the above measurements can also be considered as a test of the atomic *ab initio* calculations.

The above mentioned measurements (Hanni et al., 2008; Keele et al., 2010) were performed for Rydberg multiplets corresponding to the principal quantum numbers $n = 9..10$ by observing transitions from these levels to states with $n' = 20..21$ or $n' = 30..31$. At the same time, information about low-lying states with $l \geq 4$ is rather scarce. For instance, no g-levels are reported for Au; only 5g-levels are listed for Ag and Cu (the high Rydberg ng levels of Cu with $n = 23..28$ were studied using microwave spectroscopy (MacAdam et al., 2009)). No h-states have been reported for the above atoms. The present paper attempts to fill this gap; this is continuation of our study of the IR spectra of metals started in previous works (Civiš et al., 2010; Civiš et al., 2010, 2011).

We show that g- and h-states with $n = 5..7$ play a key role in the interpretation of the infrared spectra of Au, Ag and Cu arising in pulsed laser ablation of the metal targets in a vacuum. Some emission lines in the 2000–4000 cm^{-1} range were previously reported by us (Civiš et al., 2010; Civiš et al., 2010) with incorrect identification; after having performed the present measurements to cover the 1200–1600, 4100–5000 and 5200–7500 cm^{-1} ranges, we are able to discover the 5g-state for the gold and the 6h-states for all three metals considered. The energies of n'g- and n''h-states can easily be predicted roughly using the Rydberg formula and then refined using the measured line wavenumbers. These states allow us to give consistent classification for all lines observed in the four IR ranges mentioned.

2. Methods

In the present paper we report the IR emission spectra of Au, Ag and Cu atoms recorded using time-resolved Fourier-transform spectroscopy of the metal vapors produced during the ablation of the metal targets by a high-repetition rate (1.0 kHz) pulsed nanosecond ArF laser (λ = 193 nm, output energy of 15 mJ) in a vacuum (10^{-2} Torr). The experimental setup has already been described in detail in our previous papers (Civiš et al., 2010; Kawaguchi et al., 2008). As compared to our previous studies of the spectra of these atoms (Civiš et al., 2010; Civiš et al., 2010, 2011) this present work records their FTIR spectra in four spectral ranges (1200–1600, 1900–3600, 4100–5000 and 5200–7500 cm^{-1}). In 1200–1600 cm^{-1} range we used a high-sensitivity MCT detector that allowed us to record the spectra with a reasonable signal-to-noise ratio (SNR) as compared to the previous work (Civiš et al., 2010). For the measurements in the 1900–3600, 4100–5000 and 5200–7500 cm^{-1} ranges an InSb detector was used. Parts of the measured spectra are shown in Figure 1.

For data sampling we used the so-called 1/3 sampling, where the scanner rate was set to produce a 3 kHz HeNe laser interference signal, the ArF laser oscillation was triggered, and 30 sets of time-resolved data were recorded with a preset time interval of 1 μs. Three scans were needed for a complete interferogram, and only 5 scans were coadded to improve the SNR. The spectral resolution in such a procedure was about 0.1 cm^{-1}. We also performed measurements with only one scan but with a higher resolution of about 0.017 cm^{-1} and worse SNR. The acquired spectra were post-zerofilled (zero filling 2, trapezoid apodization function) using Bruker OPUS software and subsequently corrected by subtracting the blackbody background spectrum. The wavenumbers, line widths and their intensities (as well as the uncertainties for these quantities) were then obtained using a fitting to, *e.g.*, Gaussian line shape. For some lines we resolved their hyperfine structure. In such cases we reported each hyperfine multiplet as a single Gaussian line whose position $\bar{p}$, full width at half maximum (FWHM) $\bar{w}$ and intensity $\bar{A}$ can be obtained using the averaging procedure:

$$
\begin{aligned}
\bar{A} &= \sum A_i; \qquad \Delta\bar{A} = \left[\sum(\Delta A_i)^2\right]^{\frac{1}{2}} \\
\bar{p} &= \frac{1}{\bar{A}}\sum p_i A_i; \qquad \Delta\bar{p} = \frac{1}{\bar{A}}\left[\sum(A_i\Delta p_i)^2 + \sum(p_i-\bar{p})^2(\Delta A_i)^2\right]^{\frac{1}{2}} \\
\bar{w} &= \frac{1}{\bar{A}}\sum A_i[w_i^2 + (\bar{p}-p_i)^2] = -\bar{p}^2 + \frac{1}{\bar{A}}\sum A_i(w_i^2+p_i^2) \qquad (1) \\
\Delta\bar{w} &= \frac{1}{2\bar{w}}\left[\sum\left(\frac{\partial\bar{w}^2}{\partial w_i}\Delta w_i\right)^2 + \sum\left(\frac{\partial\bar{w}^2}{\partial p_i}\Delta p_i\right)^2 + \sum\left(\frac{\partial\bar{w}^2}{\partial A_i}\Delta A_i\right)^2\right]^{\frac{1}{2}} \\
\frac{\partial\bar{w}^2}{\partial w_i} &= \frac{2A_i w_i}{\bar{A}}; \qquad \frac{\partial\bar{w}^2}{\partial p_i} = \frac{2A_i(p_i-\bar{p})}{\bar{A}}; \qquad \frac{\partial\bar{w}^2}{\partial A_i} = \frac{(p_i-\bar{p})^2 + w_i^2 - \bar{w}^2}{\bar{A}}.
\end{aligned}
$$

Here the sum runs through all components of the multiplet; p_i, w_i and A_i are the positions, FWHMs and intensities of the multiplet components; Δ represents uncertainties. For each component these quantities were obtained by a Gaussian fitting;

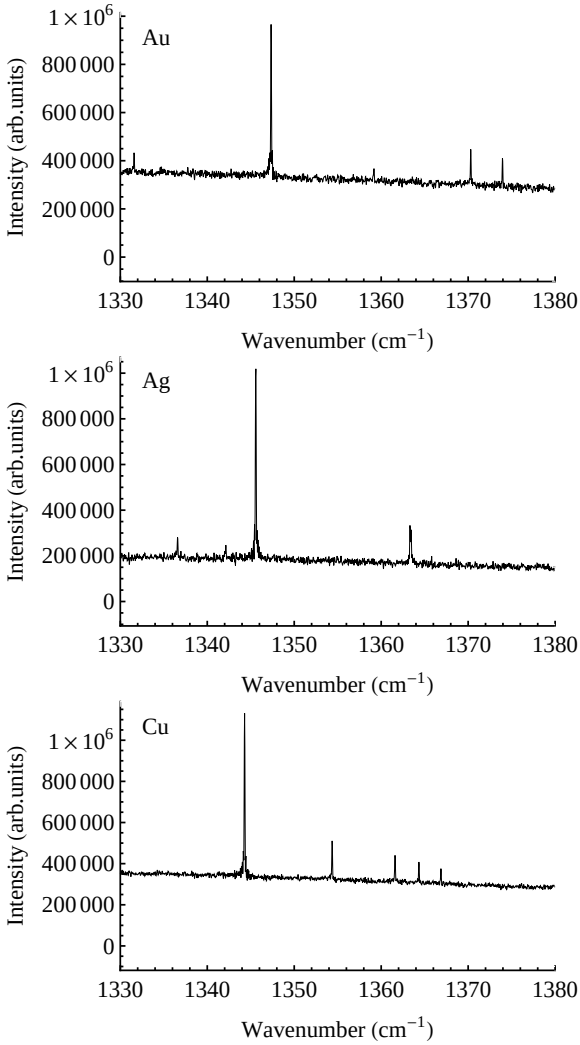

Figure 1. Emission spectra of Cu, Ag and Au in the 1330–1380 cm^{-1} range. The most prominent line (near 1345–1348 cm^{-1}) for all metals corresponds to the 5g–6h transition.

an example of such fitting of hyperfine components together with the resulting averaged lines is given in Figure 3 below. The Equations 1 have a clear physical meaning: A is determined as the area under the spectral line, $\bar{p}$ is the "center of gravity" of the multiplet, w can be considered to be proportional to the root mean square deviation.

The line identification in the present work essentially uses the dipole matrix elements (line strengths) for the transition between the $(Nd^{10})nl_j$ states of Cu ($N = 3$), Ag ($N = 4$) and Au ($N = 5$). We report here the results of the dipole transition moment calculation for gold only since the corresponding tables for silver and copper have been already published in our previous papers (Civiš et al., 2010) and (Civiš et al., 2011) correspondingly. The Fues model potential method (FMP) for these calculation was outlined in the previous paper (Civiš et al., 2010); the choice of the radial quantum number n_r (which is equal to the number of nodes of the radial wavefunction) for all the atoms under study is given in Table 1.

Table 1. Radial quantum number n_r for $(Nd^{10})nl_j$ states of Cu ($N = 3$), Ag ($N = 4$) and Au ($N = 5$) used in the Fues model potential calculation of dipole matrix elements in the present work

	$l = 0$	$l = 1$	$l = 2$	$l = 3$	$l \geq 4$
Cu	$n - 4$	$n - 4$	$n - 4$	$n - l - 1$	$n - l - 1$
Ag	$n - 5$	$n - 5$	$n - 5$	$n - l - 1$	$n - l - 1$
Au	$n - 6$	$n - 6$	$n - 5$	$n - 5$	$n - l - 1$

The procedure for extracting the energy values for the levels involved in the observed transitions is briefly described in our previous paper (Civiš et al., 2010). Since it implies a least-square fitting, it is obvious that adding new transitions to this procedure can slightly change (and, generally speaking, improve) the output results for the energy levels. Indeed, as a rule, they demonstrate slight differences (within the specified error range) from those reported in our previous studies (Civiš et al., 2010; Civiš et al., 2010, 2011) based on fewer set of observed transitions. In some cases (*e.g.*, for Au) the discrepancies are not small and they are caused by the new classification of some transitions given in the present paper, having taken into account the whole set of the observed lines. We consider these values (shown in Tables 4, 7 and 9) as recommended. All the uncertainties in the tables below are given in round brackets after the corresponding values and should be treated as their rightmost significant digits, *e. g.* 123.4(56) means 123.4 ± 5.6.

3. Results and discussion

3.1. Au

Our measurements of Au FTIR spectra were performed in three spectral regions (1200–1600, 1900–3600, 5200–7500 cm^{-1}) and this has resulted in some corrections to our previous identification (Civiš et al., 2010) of Au I levels which were based on the 1900–3600 cm^{-1} range only. The measured emission lines are presented in Table 2.

The strongest lines measured in the 5200–7500 cm^{-1} region are the 5459.12 and 5537.4 cm^{-1} lines. Together with the weaker 5454.9 cm^{-1} line, they are easily classified as due to the 6d–5f transition triplet. This yields the fine-structure splitting about 4 cm^{-1} between the $5f_{\frac{5}{2}}$ and $5f_{\frac{7}{2}}$ states. The latter value, in turn, suggests that the two strongest lines (2522.69 and 2518.49 cm^{-1}) in the 1900–3600 cm^{-1} region are due to the 5f–5g transitions. Following the first (and the only) report on the IR spectrum of gold (George et al., 1988), in our previous paper (Civiš et al., 2010) we gave another classification for these lines based on measurements in the 1800–4000 cm^{-1} range only. The present classification is essentially based on the 5g states discovered from measurements in the 5200–7500 cm^{-1} range. The correctness of the present assignment is supported by the calculations of the dipole transition matrix elements presented in Table 3. Indeed,

according to this table, the most intense lines in the 1900–3600 cm^{-1} region should correspond to the $5f_{\frac{7}{2}}$–$5g_{\frac{9}{2}}$ and $5f_{\frac{5}{2}}$–$5g_{\frac{7}{2}}$ transitions. The third component of this triplet, the $5f_{\frac{7}{2}}$–$5g_{\frac{7}{2}}$ line, has significantly low intensity and is blended by the strong 2518.49 cm^{-1} line, due to small (about 0.01 cm^{-1}, see Table 4) fine-structure splitting between the 5g levels.

The presence of only one very prominent line, 1347.34 cm^{-1}, in the 1200–1600 cm^{-1} range can be easily explained by assigning it as due to the 5g–6h transition. The triplet of possible lines is not resolved because of the small fine-structure splitting of the 5g and 6h levels. This classification is also supported by Table 3 which lists the 5g–6h transition as the most probable in the 1200–1600 cm^{-1} range (if we take into account the sum of the intensities of the three $5g_{\frac{7}{2}}$–$6h_{\frac{9}{2}}$, $5g_{\frac{9}{2}}$–$6h_{\frac{9}{2}}$ and $5g_{\frac{9}{2}}$–$6h_{\frac{11}{2}}$ lines with almost equal wavenumbers).

Given the energy levels of the 5f, 5g and 6h states, one can easily predict the energies of the nf, ng and nh levels by the extrapolation of the Rydberg formula assuming the quantum defects to be independent of n. Some levels (with $n = 6, 7$) of such a series are involved into the observed transitions, and their energies can then be determined from the measured wavenumbers. The discovery of the ng and nh levels allows us now to make some corrections to our previous classification (Civiš et al., 2010) based on emission measurements in the 1800–4000 cm^{-1} range only. The summary of corrections to the previous results are given in Table 5; and we consider the present classification as the recommended one. Some weak lines reported in the previous work were not observed in the present measurements; this could be due to different plasma conditions in two experiments. Note that there are also some differences between the line sets observed in our measurements and in the paper by George et al. (1988): we observed no lines with wavenumbers greater than 6000 cm^{-1} from those listed by George et al. (1988). In turn, in the 2100–3100 cm^{-1} range, their list lacks all lines observed in the present work except the 2518.49 cm^{-1} line. This is probably caused by the different excitation mechanisms in the hollow cathode discharge (George et al., 1988) and laser ablation experiments.

Table 4 contains the revised energy values of the Au levels obtained from the present measurement in three spectral ranges. The majority of the energies are close to the previously reported values. The most significant discrepancy (about 8 cm^{-1}) is found for the $5f_{\frac{5}{2}}$ term whose energy value was reported 70 years ago (Platt and Sawyer, 1941). Together with the incorrect classification of the 2518.49 cm^{-1} line, this old-reported energy value has caused some problems with discrepancies between the measured and calculated wavenumbers in the paper by George et al. (1988, bottom of p. 1501). With our new classification involving g and h-states, the observed set of lines and levels seems to be self-consistent and we consider the energy values of the levels presented in Table 4 to be the recommended ones.

Table 2. Au I lines and their identification. Each of the four spectral ranges (1200–1600, 1900–3600, 4100–5000 and 5200–7500 cm^{-1}) has its own scale of arbitrary units for the emission intensity.

Wavenumber (cm^{-1})	Intensity (arb. units)	SNR	FWHM (cm^{-1})	Identification
1289.364(8)	1.08×10^4	11.1	0.068(20)	$9s_{\frac{1}{2}}$–$9p_{\frac{3}{2}}$
1331.582(9)	1.10×10^4	7.33	0.086(28)	$8d_{\frac{5}{2}}$–$7f_{\frac{7}{2}}$
1347.3390(7)	1.00×10^5	30.7	0.023(2)	5g –6h
1370.302(3)	2.18×10^4	18.1	0.028(9)	$8d_{\frac{3}{2}}$–$7f_{\frac{5}{2}}$
1373.952(5)	1.53×10^4	13.8	0.023(14)	$6f_{\frac{5}{2}}$–$6g_{\frac{7}{2}}$
2156.521(11)	1.80×10^4	4.43	0.065(39)	5g –7h
2174.019(3)	1.77×10^4	6.48	0.033(11)	$\left[\left(5d^9_{\frac{3}{2}}\,6s\right)_2 6p_{\frac{3}{2}}\right]_{\frac{1}{2}}$–$8s_{\frac{1}{2}}$
2178.742(2)	1.61×10^4	14.5	0.019(4)	$7d_{\frac{3}{2}}$–$9p_{\frac{1}{2}}$
2180.650(12)	1.82×10^4	5.93	0.081(41)	$6f_{\frac{7}{2}}$–$7g_{\frac{9}{2}}$
2184.294(13)	1.06×10^4	4.67	0.067(42)	$6f_{\frac{5}{2}}$–$7g_{\frac{7}{2}}$
2193.0300(5)	1.26×10^5	62.7	0.031(1)	$8s_{\frac{1}{2}}$–$8p_{\frac{1}{2}}$
2459.403(3)	1.29×10^4	10.3	0.028(8)	$7d_{\frac{5}{2}}$–$9p_{\frac{3}{2}}$
2471.304(2)	1.70×10^4	13.9	0.028(6)	$7d_{\frac{5}{2}}$–$6f_{\frac{5}{2}}$
2474.9613(4)	6.07×10^5	82.6	0.046(1)	$7d_{\frac{5}{2}}$–$6f_{\frac{7}{2}}$
2484.120(2)	1.40×10^4	12.8	0.029(7)	$8p_{\frac{3}{2}}$–$8d_{\frac{3}{2}}$
2512.2183(3)	4.11×10^5	91.3	0.044(1)	$7d_{\frac{3}{2}}$–$6f_{\frac{5}{2}}$
2518.4851(2)	1.49×10^6	265.	0.037(1)	$5f_{\frac{7}{2}}$–$5g_{\frac{9}{2}}$
2520.6809(5)	2.08×10^5	60.0	0.044(2)	$8p_{\frac{3}{2}}$–$8d_{\frac{5}{2}}$
2522.6828(3)	1.13×10^6	131.	0.035(1)	$5f_{\frac{5}{2}}$–$5g_{\frac{7}{2}}$
2744.3848(3)	3.47×10^5	150.	0.040(1)	$8s_{\frac{1}{2}}$–$8p_{\frac{3}{2}}$
3035.474(1)	5.49×10^4	27.6	0.044(3)	$8p_{\frac{1}{2}}$–$8d_{\frac{3}{2}}$
3179.051(2)	2.11×10^4	11.5	0.025(6)	$\left[\left(5d^9_{\frac{3}{2}}\,6s\right)_1 6p_{\frac{3}{2}}\right]_{\frac{1}{2}}$–$8s_{\frac{1}{2}}$
3187.8097(9)	4.13×10^4	17.2	0.032(3)	$\left[\left(5d^9_{\frac{3}{2}}\,6s\right)_2 6p_{\frac{1}{2}}\right]_{\frac{3}{2}}$–$6d_{\frac{5}{2}}$
4463.816(21)	9.76×10^4	8.47	0.283(66)	$\left[\left(5d^9_{\frac{3}{2}}\,6s\right)_2 6p_{\frac{3}{2}}\right]_{\frac{3}{2}}$–$7d_{\frac{3}{2}}$
4504.725(9)	1.09×10^6	7.34	0.282(34)	$\left[\left(5d^9_{\frac{3}{2}}\,6s\right)_2 6p_{\frac{3}{2}}\right]_{\frac{3}{2}}$–$7d_{\frac{5}{2}}$
4644.939(13)	6.48×10^4	7.11	0.120(40)	$7d_{\frac{5}{2}}$–$8f_{\frac{7}{2}}$
4672.724(10)	9.40×10^4	12.7	0.141(30)	$5f_{\frac{7}{2}}$–$7g_{\frac{9}{2}}$
4676.968(11)	3.51×10^4	7.55	0.087(36)	$5f_{\frac{5}{2}}$–$7g_{\frac{7}{2}}$
4688.344(12)	5.17×10^4	8.94	0.115(38)	$7d_{\frac{3}{2}}$–$8f_{\frac{5}{2}}$
4709.816(3)	4.62×10^5	23.2	0.124(10)	$7p_{\frac{1}{2}}$–$8s_{\frac{1}{2}}$
4900.786(8)	8.96×10^4	15.4	0.131(24)	$\left[\left(5d^9_{\frac{3}{2}}\,6s\right)_2 6p_{\frac{3}{2}}\right]_{\frac{1}{2}}$–$7d_{\frac{3}{2}}$
4984.048(5)	1.20×10^5	18.3	0.116(15)	$6d_{\frac{3}{2}}$–$8p_{\frac{1}{2}}$
5227.367(10)	2.63×10^4	8.82	0.082(30)	$8s_{\frac{1}{2}}$–$9p_{\frac{3}{2}}$
5454.902(3)	3.18×10^4	9.45	0.029(7)	$6d_{\frac{5}{2}}$–$5f_{\frac{5}{2}}$
5459.1214(5)	1.06×10^6	22.3	0.039(2)	$6d_{\frac{5}{2}}$–$5f_{\frac{7}{2}}$
5537.3925(4)	6.70×10^5	35.3	0.038(1)	$6d_{\frac{3}{2}}$–$5f_{\frac{5}{2}}$
5547.842(8)	2.20×10^4	5.89	0.087(22)	$7s_{\frac{1}{2}}$–$7p_{\frac{1}{2}}$
5896.366(9)	3.95×10^4	10.7	0.118(24)	$\left[\left(5d^9_{\frac{3}{2}}\,6s\right)_2 6p_{\frac{1}{2}}\right]_{\frac{3}{2}}$–$8s_{\frac{1}{2}}$
5905.855(6)	2.86×10^4	20.1	0.078(33)	$\left[\left(5d^9_{\frac{3}{2}}\,6s\right)_1 6p_{\frac{3}{2}}\right]_{\frac{3}{2}}$–$7d_{\frac{3}{2}}$
7118.816(14)	2.17×10^4	5.55	0.061(41)	$\left[\left(5d^9_{\frac{3}{2}}\,6s\right)_1 6p_{\frac{3}{2}}\right]_{\frac{3}{2}}$–$9s_{\frac{1}{2}}$
7436.611(6)	2.70×10^4	10.6	0.102(18)	$7p_{\frac{1}{2}}$–$7d_{\frac{3}{2}}$

Table 3: FMP-calculated transition dipole moments (line strengths S_{ik}, oscillator strengths f_{ik}, transition probabilities A_{ki}) between the $5d^{10}$ states of the Au atom observed in the present work. The energies of all levels are taken from the present measurement (see Table 4) except that for the $7p_{\frac{3}{2}}$ level (taken from George et al., 1988) and $6g_{\frac{9}{2}}$ levels (extrapolated from the values reported in Table 4). The Ritz wavenumbers ν and air wavelengths λ are calculated using these energy values.

Transition i–k	Lower level (cm^{-1})	Upper level (cm^{-1})	ν (cm^{-1})	λ (nm)	S_{ik} (a. u.)	f_{ik}	A_{ki} (s^{-1})
$6g_{\frac{9}{2}}$–$8f_{\frac{7}{2}}$	71355.890	72155.539	799.649	12502.1	9.78×10^{1}	2.38×10^{-2}	1.27×10^{4}
$6g_{\frac{7}{2}}$–$8f_{\frac{7}{2}}$	71355.845	72155.539	799.694	12501.4	2.79	8.48×10^{-4}	3.62×10^{2}
$6g_{\frac{7}{2}}$–$8f_{\frac{5}{2}}$	71355.845	72158.019	802.174	12462.7	7.22×10^{1}	2.20×10^{-2}	1.26×10^{4}
$6g_{\frac{9}{2}}$–$7h_{\frac{11}{2}}$	71355.890	72168.489	812.599	12302.8	5.91×10^{3}	1.46	5.36×10^{5}
$6g_{\frac{9}{2}}$–$7h_{\frac{9}{2}}$	71355.890	72168.489	812.599	12302.8	1.10×10^{2}	2.70×10^{-2}	1.19×10^{4}
$6g_{\frac{7}{2}}$–$7h_{\frac{9}{2}}$	71355.845	72168.489	812.644	12302.2	4.82×10^{3}	1.49	5.24×10^{5}
$9s_{\frac{1}{2}}$–$9p_{\frac{1}{2}}$	68680.631	69648.344	967.713	10330.8	4.48×10^{2}	6.58×10^{-1}	4.11×10^{5}
$8p_{\frac{3}{2}}$–$9s_{\frac{1}{2}}$	67487.264	68680.631	1193.367	8377.37	5.23×10^{2}	4.74×10^{-1}	9.00×10^{5}
$9s_{\frac{1}{2}}$–$9p_{\frac{3}{2}}$	68680.631	69969.927	1289.296	7754.06	6.64×10^{2}	1.30	7.21×10^{5}
$5g_{\frac{9}{2}}$–$7f_{\frac{7}{2}}$	70011.968	71339.538	1327.570	7530.51	2.20×10^{1}	8.89×10^{-3}	1.31×10^{4}
$5g_{\frac{7}{2}}$–$7f_{\frac{7}{2}}$	70011.96	71339.538	1327.578	7530.46	6.30×10^{-1}	3.17×10^{-4}	3.73×10^{2}
$5g_{\frac{7}{2}}$–$7f_{\frac{5}{2}}$	70011.96	71341.709	1329.749	7518.17	1.66×10^{1}	8.38×10^{-3}	1.32×10^{4}
$8d_{\frac{5}{2}}$–$7f_{\frac{7}{2}}$	70007.956	71339.538	1331.582	7507.82	2.17×10^{3}	1.47	1.30×10^{6}
$8d_{\frac{5}{2}}$–$7f_{\frac{5}{2}}$	70007.956	71341.709	1333.753	7495.60	1.08×10^{2}	7.30×10^{-2}	8.66×10^{4}
$5g_{\frac{9}{2}}$–$6h_{\frac{11}{2}}$	70011.968	71359.307	1347.339	7420.01	4.02×10^{3}	1.65	1.66×10^{6}
$5g_{\frac{9}{2}}$–$6h_{\frac{9}{2}}$	70011.968	71359.307	1347.339	7420.01	7.45×10^{1}	3.05×10^{-2}	3.69×10^{4}
$5g_{\frac{7}{2}}$–$6h_{\frac{9}{2}}$	70011.96	71359.307	1347.347	7419.97	3.28×10^{3}	1.68	1.62×10^{6}
$8d_{\frac{3}{2}}$–$7f_{\frac{5}{2}}$	69971.407	71341.709	1370.302	7295.67	1.41×10^{3}	1.47	1.22×10^{6}
$8p_{\frac{1}{2}}$–$9s_{\frac{1}{2}}$	66935.902	68680.631	1744.729	5729.99	1.70×10^{2}	4.51×10^{-1}	9.16×10^{5}
$7p_{\frac{1}{2}}$–$6d_{\frac{3}{2}}$	60033.076	61951.885	1918.809	5210.15	1.65×10^{2}	4.81×10^{-1}	5.90×10^{5}
$5g_{\frac{9}{2}}$–$8f_{\frac{7}{2}}$	70011.968	72155.539	2143.571	4663.84	2.15	1.40×10^{-3}	5.36×10^{3}
$5g_{\frac{7}{2}}$–$8f_{\frac{7}{2}}$	70011.96	72155.539	2143.579	4663.82	6.14×10^{-2}	5.00×10^{-5}	1.53×10^{2}
$5g_{\frac{7}{2}}$–$8f_{\frac{5}{2}}$	70011.96	72158.019	2146.059	4658.43	1.60	1.30×10^{-3}	5.33×10^{3}
$8d_{\frac{5}{2}}$–$8f_{\frac{7}{2}}$	70007.956	72155.539	2147.583	4655.13	2.51×10^{2}	2.73×10^{-1}	6.29×10^{5}
$8d_{\frac{5}{2}}$–$8f_{\frac{5}{2}}$	70007.956	72158.019	2150.063	4649.76	1.26×10^{1}	1.37×10^{-2}	4.22×10^{4}
$5g_{\frac{9}{2}}$–$7h_{\frac{11}{2}}$	70011.968	72168.489	2156.521	4635.83	3.05×10^{2}	2.00×10^{-1}	5.16×10^{5}
$5g_{\frac{9}{2}}$–$7h_{\frac{9}{2}}$	70011.968	72168.489	2156.521	4635.83	5.64	3.70×10^{-3}	1.15×10^{4}

Transition i–k	Lower level (cm^{-1})	Upper level (cm^{-1})	ν (cm^{-1})	λ (nm)	S_{ik} (a. u.)	f_{ik}	A_{ki} (s^{-1})
$5g_{\frac{7}{2}}$–$7h_{\frac{9}{2}}$	70011.96	72168.489	2156.529	4635.82	2.48×10^{2}	2.03×10^{-1}	5.05×10^{5}
$7d_{\frac{3}{2}}$–$9p_{\frac{1}{2}}$	67469.675	69648.344	2178.669	4588.71	1.47×10^{2}	2.43×10^{-1}	1.54×10^{6}
$8d_{\frac{3}{2}}$–$8f_{\frac{5}{2}}$	69971.407	72158.019	2186.612	4572.04	1.76×10^{2}	2.93×10^{-1}	6.23×10^{5}
$8s_{\frac{1}{2}}$–$8p_{\frac{1}{2}}$	64742.879	66935.902	2193.023	4558.67	1.58×10^{2}	5.26×10^{-1}	1.69×10^{6}
$7d_{\frac{5}{2}}$–$9p_{\frac{3}{2}}$	67510.6	69969.927	2459.327	4065.04	1.09×10^{2}	1.35×10^{-1}	8.19×10^{5}
$7d_{\frac{5}{2}}$–$6f_{\frac{5}{2}}$	67510.6	69981.893	2471.293	4045.36	6.12×10^{1}	7.66×10^{-2}	3.12×10^{5}
$7d_{\frac{5}{2}}$–$6f_{\frac{7}{2}}$	67510.6	69985.563	2474.963	4039.36	1.22×10^{3}	1.53	4.69×10^{6}
$5f_{\frac{5}{2}}$–$8d_{\frac{3}{2}}$	67489.277	69971.407	2482.130	4027.70	9.06×10^{-1}	1.14×10^{-3}	7.02×10^{3}
$8p_{\frac{3}{2}}$–$8d_{\frac{3}{2}}$	67487.264	69971.407	2484.143	4024.44	1.14×10^{1}	2.15×10^{-2}	8.83×10^{4}
$7d_{\frac{3}{2}}$–$9p_{\frac{3}{2}}$	67469.675	69969.927	2500.252	3998.51	1.10×10^{1}	2.09×10^{-2}	8.70×10^{4}
$7d_{\frac{3}{2}}$–$6f_{\frac{5}{2}}$	67469.675	69981.893	2512.218	3979.46	8.31×10^{2}	1.58	4.45×10^{6}
$5f_{\frac{7}{2}}$–$8d_{\frac{5}{2}}$	67493.483	70007.956	2514.473	3975.89	7.48×10^{-1}	7.14×10^{-4}	4.01×10^{3}
$5f_{\frac{7}{2}}$–$5g_{\frac{7}{2}}$	67493.483	70011.96	2518.477	3969.57	3.90×10^{1}	3.73×10^{-2}	1.58×10^{5}
$5f_{\frac{7}{2}}$–$5g_{\frac{9}{2}}$	67493.483	70011.968	2518.485	3969.56	1.37×10^{3}	1.31	4.42×10^{6}
$5f_{\frac{5}{2}}$–$8d_{\frac{5}{2}}$	67489.277	70007.956	2518.679	3969.25	3.60×10^{-2}	4.59×10^{-5}	1.94×10^{2}
$8p_{\frac{3}{2}}$–$8d_{\frac{5}{2}}$	67487.264	70007.956	2520.692	3966.08	8.80×10^{1}	1.68×10^{-1}	4.76×10^{5}
$5f_{\frac{5}{2}}$–$5g_{\frac{7}{2}}$	67489.277	70011.96	2522.683	3962.95	1.05×10^{3}	1.34	4.28×10^{6}
$8s_{\frac{1}{2}}$–$8p_{\frac{3}{2}}$	64742.879	67487.264	2744.385	3642.81	2.47×10^{2}	1.03	2.58×10^{6}
$8p_{\frac{1}{2}}$–$8d_{\frac{3}{2}}$	66935.902	69971.407	3035.505	3293.45	1.18×10^{1}	5.42×10^{-2}	1.67×10^{5}
$7d_{\frac{5}{2}}$–$7f_{\frac{7}{2}}$	67510.6	71339.538	3828.938	2610.98	1.14×10^{2}	2.21×10^{-1}	1.62×10^{6}
$7d_{\frac{5}{2}}$–$7f_{\frac{5}{2}}$	67510.6	71341.709	3831.109	2609.50	5.73	1.11×10^{-2}	1.09×10^{5}
$5f_{\frac{7}{2}}$–$6g_{\frac{7}{2}}$	67493.483	71355.845	3862.362	2588.38	3.56	5.21×10^{-3}	5.19×10^{4}
$5f_{\frac{7}{2}}$–$6g_{\frac{9}{2}}$	67493.483	71355.890	3862.407	2588.35	1.24×10^{2}	1.82×10^{-1}	1.45×10^{6}
$5f_{\frac{5}{2}}$–$6g_{\frac{7}{2}}$	67489.277	71355.845	3866.568	2585.57	9.62×10^{1}	1.88×10^{-1}	1.41×10^{6}
$7d_{\frac{3}{2}}$–$7f_{\frac{5}{2}}$	67469.675	71341.709	3872.034	2581.92	8.16×10^{1}	2.40×10^{-1}	1.60×10^{6}
$5f_{\frac{7}{2}}$–$7g_{\frac{9}{2}}$	67493.483	72166.209	4672.726	2139.49	3.33×10^{1}	5.91×10^{-2}	6.88×10^{5}
$5f_{\frac{7}{2}}$–$7g_{\frac{7}{2}}$	67493.483	72166.221	4672.738	2139.49	9.51×10^{-1}	1.69×10^{-3}	2.46×10^{4}
$5f_{\frac{5}{2}}$–$7g_{\frac{7}{2}}$	67489.277	72166.221	4676.944	2137.56	2.58×10^{1}	6.10×10^{-2}	6.68×10^{5}
$7p_{\frac{1}{2}}$–$8s_{\frac{1}{2}}$	60033.076	64742.879	4709.803	2122.65	4.03×10^{1}	2.88×10^{-1}	4.26×10^{6}
$8s_{\frac{1}{2}}$–$9p_{\frac{1}{2}}$	64742.879	69648.344	4905.465	2037.99	1.54	1.15×10^{-2}	1.84×10^{5}
$6d_{\frac{3}{2}}$–$8p_{\frac{1}{2}}$	61951.885	66935.902	4984.017	2005.87	3.95×10^{1}	1.49×10^{-1}	4.95×10^{6}
$8s_{\frac{1}{2}}$–$9p_{\frac{3}{2}}$	64742.879	69969.927	5227.048	1912.60	1.02×10^{1}	8.08×10^{-2}	7.36×10^{5}
$6d_{\frac{5}{2}}$–$8p_{\frac{3}{2}}$	62034.361	67487.264	5452.903	1833.38	3.22×10^{1}	8.90×10^{-2}	2.65×10^{6}
$6d_{\frac{5}{2}}$–$5f_{\frac{5}{2}}$	62034.361	67489.277	5454.916	1832.71	2.76×10^{1}	7.62×10^{-2}	1.51×10^{6}
$6d_{\frac{5}{2}}$–$5f_{\frac{7}{2}}$	62034.361	67493.483	5459.122	1831.30	5.52×10^{2}	1.52	2.27×10^{7}
$6d_{\frac{3}{2}}$–$8p_{\frac{3}{2}}$	61951.885	67487.264	5535.379	1806.07	3.30	1.39×10^{-2}	2.84×10^{5}
$6d_{\frac{3}{2}}$–$5f_{\frac{5}{2}}$	61951.885	67489.277	5537.392	1805.41	3.80×10^{2}	1.60	2.18×10^{7}

Transition i–k	Lower level (cm^{-1})	Upper level (cm^{-1})	ν (cm^{-1})	λ (nm)	S_{ik} (a. u.)	f_{ik}	A_{ki} (s^{-1})
$7s_{\frac{1}{2}}$–$7p_{\frac{1}{2}}$	54485.235	60033.076	5547.841	1802.01	4.26×10^{1}	3.59×10^{-1}	7.37×10^{6}
$7p_{\frac{1}{2}}$–$7d_{\frac{3}{2}}$	60033.076	67469.675	7436.599	1344.33	1.29	1.46×10^{-2}	2.69×10^{5}

3.2. Ag

The emission spectra of Ag were recorded in the three ranges, 1200–1600 cm^{-1}, 4100–5000 cm^{-1} and 5200–7500 cm^{-1}. Only for the latter range have we found an earlier (but century-old) study (Randall, 1911) of Ag lines which reported four lines: 5438.6, 5460.7, 5740.0 and 5943.9 cm^{-1}. Our results (six lines in Table 6 below) display some differences but obviously have a much higher accuracy, which made it for us possible to resolve the fine structure of the 4f states.

Indeed, our previous measurement (Civiš et al., 2010) has shown that the fine splitting of the f-states in Ag is quite small (0.122 cm^{-1} and 0.245 cm^{-1} for the 5f and 7f states correspondingly) and that it is considerable low as compared to the fine-structure splitting of the f-states in Au and Cu. The fine structure of the 4f state in Ag remained unresolved. We noted (Civiš et al., 2010) that, to obtain reliable values of the fine-splitting component of the 4f levels, one should consider the transitions from these states to nd states, since the latter have larger fine-structure splitting. Such transitions (with $n = 5$) have been observed in the present work in the 5200–7500 cm^{-1} range and this allowed us to resolve the fine structure for 4f state. We have also resolved this for the 6g state, using the 5f–6g doublet measured at 1363 cm^{-1}. Unfortunately, our data is still not sufficient to resolve the fine structure of the 5g state from the most prominent 2506 cm^{-1} line since, due to its high intensity and comparatively large width, it cannot be reliably fitted by a two-peak curve. We show this line together with the less intensive 1363 cm^{-1} doublet in Figure 2.

The present measurements in the 1200–1600 cm^{-1} range also help us to resolve some problems with line identification in the previous measurement (Civiš et al., 2010) using a low-sensitive MCT detector resulting in a high noise level. We are able to observe the 7d–6f doublet at 1336.6 and 1342.15 cm^{-1} while the most prominent 1345.6 cm^{-1} line (incorrectly classified as due to the $7d_{\frac{3}{2}}$–$6f_{\frac{5}{2}}$ transition (Civiš et al., 2010)) corresponds to the 5g–5h transition, similarly as in the case of Au.

Table 7 presents the energies of the Ag levels involved in the observed transitions. Their uncertainties are lower than those for Au and Cu (see Table 9 below), since for the Ag levels we used the high-accuracy reference values published by Pickering and Zilio (2001). Most of the values do not differ much from the previous measurement (Civiš et al., 2010) and from other sources. The exception is the $6f_{\frac{5}{2}}$ level whose value was extracted using an incorrect identification of the 1345.6 cm^{-1} line (Civiš et al., 2010). We did not include in this table some levels for which we have obtained here exactly the same values as reported in the previous work (Civiš et al., 2010).

Table 4. Revised values of some levels of Au I

Term	Energy (cm^{-1})	Other sources
$5d^{10}\,7h$	72168.489(37)	This work
$5d^{10}\,7g_{\frac{9}{2}}$	72166.211(47)	This work
$5d^{10}\,7g_{\frac{7}{2}}$	72166.188(45)	This work
$5d^{10}\,6h$	71359.307(35)	This work
$5d^{10}\,6g_{\frac{7}{2}}$	71355.845(43)	This work
$5d^{10}\,7f_{\frac{5}{2}}$	71341.709(40)	This work
$5d^{10}\,7f_{\frac{7}{2}}$	71339.538(34)	71339.569[a]
$5d^{10}\,5g_{\frac{9}{2}}$	70011.968(35)	This work
$5d^{10}\,5g_{\frac{7}{2}}$	70011.960(47)	This work
$5d^{10}\,8d_{\frac{5}{2}}$	70007.956(33)	70007.6[b] , 70007.975[c]
$5d^{10}\,6f_{\frac{7}{2}}$	69985.561(45)	69985.559[a]
$5d^{10}\,6f_{\frac{5}{2}}$	69981.893(43)	69988.172[a]
$5d^{10}\,8d_{\frac{3}{2}}$	69971.407(40)	69971.3[b] , 69971.418[c]
$5d^{10}\,9p_{\frac{3}{2}}$	69969.926(94)	69969.89[d] , 69967.489[a]
$5d^{10}\,9p_{\frac{1}{2}}$	69648.345(75)	69648.28[d] , 69950.681[a]
$5d^{10}\,9s_{\frac{1}{2}}$	68680.631(50)	68680.5[b] , 68680.628[c]
$5d^{10}\,7d_{\frac{5}{2}}$	67510.600(45)	67510.7[b] , 67510.605[c]
$5d^{10}\,5f_{\frac{5}{2}}$	67489.277(47)	67490.0[b] , 67489.276[f] , 67491.487[a]
$5d^{10}\,5f_{\frac{7}{2}}$	67493.483(35)	67485.3[b] , 67485.292[a]
$5d^{10}\,7d_{\frac{3}{2}}$	67469.675(44)	67469.4[b] , 67469.683[c]
$5d^{10}\,8p_{\frac{3}{2}}$	67487.264(29)	67487.11[d] , 67487.291[a]
$5d^{10}\,8p_{\frac{1}{2}}$	66935.902(29)	66935.76[d] , 66935.941[a]
$5d^{10}\,8s_{\frac{1}{2}}$	64742.879(29)	64742.4[b] , 64742.896[c] , 64742.911[a]
$\left[\left(5d^9_{\frac{3}{2}}\,6s\right)_2\,6p_{\frac{3}{2}}\right]_{\frac{3}{2}}$	63005.873(38)	63005.1[b] (20° state), 63005.7[e] (J series, $n = 6$), 63005.883[f]
$\left[\left(5d^9_{\frac{3}{2}}\,6s\right)_2\,6p_{\frac{3}{2}}\right]_{\frac{1}{2}}$	62568.757(131)	62568.7[e] (I series, $n = 6$)
$5d^{10}\,6d_{\frac{5}{2}}$	62034.361(35)	62033.7[b] , 62034.363[c]
$5d^{10}\,6d_{\frac{3}{2}}$	61951.885(48)	61951.6[b] , 61951.886[c]
$\left[\left(5d^9_{\frac{3}{2}}\,6s\right)_1\,6p_{\frac{3}{2}}\right]_{\frac{3}{2}}$	61563.839(20)	61563.840[f] , 61563.7[e] (E series, $n = 6$), 61563.3[b] (19° state)
$5d^{10}\,7p_{\frac{1}{2}}$	60033.076(20)	60033.0[b] , 60032.85[d] , 60033.076[f]
$\left[\left(5d^9_{\frac{3}{2}}\,6s\right)_2\,6p_{\frac{1}{2}}\right]_{\frac{3}{2}}$	58846.546(19)	58845.1[b] (16° state), 58845.414[c] (16° state), 58846.4[e] (H series, $n = 6$), 58846.546[f]
$5d^{10}\,7s_{\frac{1}{2}}$	54485.235(50)	54484.9[b] , 54485.235[c]

[a] (Civiš et al., 2010)
[b] (Platt and Sawyer, 1941)
[c] (Ehrhardt and Davis, 1971)
[d] (Brown and Ginter, 1978)
[e] (Jannitti et al., 1979)
[f] (George et al., 1988)

Table 5. A summary of corrections to the previous results (Civiš et al., 2010) for the classification of Au lines in the 1900–3600 range

Wavenumber (cm^{-1})	Previous	Present
2156.48	$8d_{\frac{5}{2}}$–$8f_{\frac{7}{2}}$	5g–7h
2428.36	$9p_{\frac{3}{2}}$–$12s_{\frac{1}{2}}$	not observed
2512.22	$9p_{\frac{1}{2}}$–$10d_{\frac{3}{2}}$	$7d_{\frac{3}{2}}$–$6f_{\frac{5}{2}}$
2518.49	$5f_{\frac{7}{2}}$–$8d_{\frac{5}{2}}$ [a], $7d_{\frac{3}{2}}$–$6f_{\frac{5}{2}}$	$5f_{\frac{7}{2}}$–$5g_{\frac{9}{2}}$
2522.69	$5f_{\frac{7}{2}}$–$8d_{\frac{5}{2}}$	$5f_{\frac{5}{2}}$–$5g_{\frac{7}{2}}$
2743.37	not classified	not observed
2747.57	$9p_{\frac{1}{2}}$–$12s_{\frac{1}{2}}$	not observed
2749.6	$9d_{\frac{3}{2}}$–23p	not observed

[a] George et al. (1988)

Table 6. Ag I lines and their identification. Each of the three spectral ranges, 1200–1600 cm^{-1}, 4100–5000 cm^{-1} and 5200–7500 cm^{-1}, has its own scale of arbitrary units for the emission intensity.

Wavenumber (cm^{-1})	Intensity (arb. units)	SNR	FWHM (cm^{-1})	Identification
1336.596(3)	1.91×10^{3}	9.85	0.032(9)	$7d_{\frac{5}{2}}$–$6f_{\frac{7}{2}}$
1342.154(4)	1.53×10^{3}	7.42	0.032(10)	$7d_{\frac{3}{2}}$–$6f_{\frac{5}{2}}$
1345.5757(4)	1.81×10^{4}	54.9	0.033(1)	5g–6h
1363.315(2)	3.06×10^{3}	12.7	0.029(5)	$5f_{\frac{7}{2}}$–$6g_{\frac{9}{2}}$
1363.435(3)	3.14×10^{3}	8.63	0.042(8)	$5f_{\frac{5}{2}}$–$6g_{\frac{7}{2}}$
1392.791(7)	6.51×10^{3}	7.94	0.061(30)	$8p_{\frac{3}{2}}$–$8d_{\frac{5}{2}}$
1460.111(1)	1.73×10^{3}	19.3	0.018(3)	$7p_{\frac{3}{2}}$–$8s_{\frac{1}{2}}$
4241.535(8)	1.63×10^{4}	8.56	0.071(28)	$5p_{\frac{3}{2}}$–$4d^{9}\,5s^{2}\left(^{2}D_{\frac{3}{2}}\right)$
4356.957(17)	1.72×10^{4}	5.07	0.093(52)	$7p_{\frac{3}{2}}$–$10s_{\frac{1}{2}}$
4659.898(6)	2.15×10^{5}	20.9	0.122(9)	4f–7g
4743.434(11)	3.67×10^{4}	6.42	0.092(35)	$7p_{\frac{3}{2}}$–$9d_{\frac{5}{2}}$
4773.611(4)	1.05×10^{5}	27.1	0.101(13)	$7s_{\frac{1}{2}}$–$8p_{\frac{3}{2}}$
5440.5263(4)	1.68×10^{6}	41.5	0.041(1)	$5d_{\frac{5}{2}}$–$4f_{\frac{7}{2}}$
5460.7604(4)	9.06×10^{5}	76.5	0.041(1)	$5d_{\frac{3}{2}}$–$4f_{\frac{5}{2}}$
5712.7521(6)	4.73×10^{5}	55.2	0.038(2)	$6p_{\frac{3}{2}}$–$6d_{\frac{5}{2}}$
5741.2630(7)	6.70×10^{5}	45.3	0.041(2)	$6s_{\frac{1}{2}}$–$6p_{\frac{1}{2}}$
5905.714(1)	2.02×10^{5}	27.6	0.037(3)	$6p_{\frac{1}{2}}$–$6d_{\frac{3}{2}}$
5944.6650(5)	9.83×10^{5}	55.5	0.039(1)	$6s_{\frac{1}{2}}$–$6p_{\frac{3}{2}}$

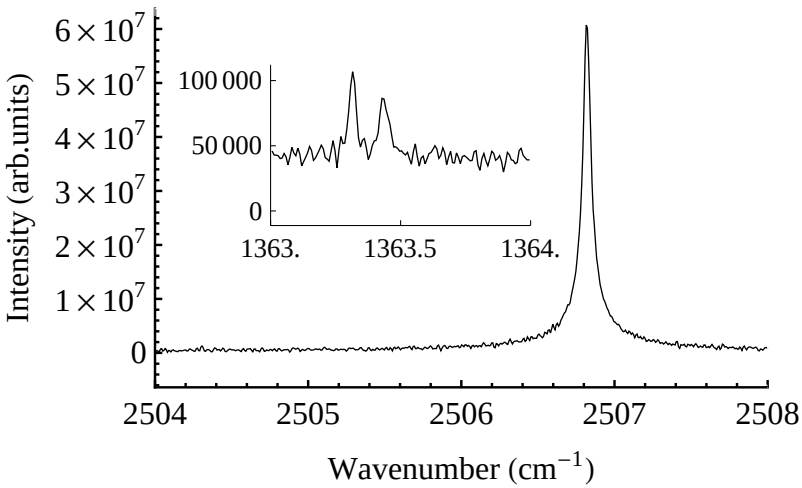

Figure 2. The 4f–5g (2506.82 cm^{-1}) line with non-resolved fine-splitting structure and $5f_{\frac{7}{2}}$–$6g_{\frac{9}{2}}$ & $5f_{\frac{5}{2}}$–$6g_{\frac{7}{2}}$ doublet (1362 cm^{-1}) in Ag I. The arbitrary units for intensity have different scales on vertical axes in the inset and in the main graph.

3.3. Cu

To our knowledge, the only study of the Cu spectrum in the 5200–7500 cm^{-1} range was reported about 60 years ago (Shenstone, 1948) where four (5484.1, 5496.6, 6003.2 and 6245.0 cm^{-1}) lines were mentioned. Our measurement yielded 8 lines (see Table 8 below) which can be easily classified as consisting of two triplets (4d–4f and 5p–5d) and the 5s–5p doublet. The latter consists of two very close lines which are due to the small (about 0.3 cm^{-1}) fine-structure splitting of the 5p term of Cu I. This doublet is shown in Figure 3; the hyperfine structure is clearly seen. The reported (Table 8) parameters of such multiplets are averaged over the hyperfine structure according to Equations 1.

Similarly to Au and Ag, the most prominent line (1344 cm^{-1}) of Cu in the 1200–1600 cm^{-1} range is due to the 5g–6h transition. The 1277 and 1302 cm^{-1} lines are easily identified using energy values taken from the literature. The remaining four lines are identified as being due to the two most prominent pairs of the 5f–6g and 6d–6f triplets; this identification is based on a comparison of the corresponding line strengths calculated using the FMP method. The information about the 6h term extracted from the measurements in the 1200–1600 cm^{-1} region makes it possible for us to identify the 2153 cm^{-1} line (not reported in the previous work (Civiš et al., 2011)) as due to the 5g–7h transition.

The revised Cu I level energies using the present measurements are given in Table 9. For the majority of levels, the difference between the results reported in this and in other works is of the same order of magnitude as the uncertainty specified. Nevertheless, the present values of the $6g_{\frac{7}{2},\frac{9}{2}}$ levels differ by almost 0.6 cm^{-1} as compared to our previous work (Civiš et al., 2011). We consider the present values to be preferable since these are extracted here from stronger lines (1354 and 1361 cm^{-1}) while the previous work used the less prominent 3837 and 3840 cm^{-1} lines which lie at the boundary of the

Table 7. Revised values of some levels of Ag I

Term	Energy (cm^{-1})	Other sources
$4d^{10}\,7g$	58864.644(7)	This work
$4d^{10}\,9d_{\frac{5}{2}}$	58864.603(16)	58864.614 (Pickering and Zilio, 2001)
$4d^{10}\,10s_{\frac{1}{2}}$	58478.051(30)	58478.047 (Pickering and Zilio, 2001)
$4d^{10}\,6h$	58057.140(4)	This work
$4d^{10}\,6g_{\frac{9}{2}}$	58054.713(3)	58054.723 (Civiš et al., 2010)
$4d^{10}\,6g_{\frac{7}{2}}$	58054.711(4)	58054.723 (Civiš et al., 2010)
$4d^{10}\,8d_{\frac{5}{2}}$	58053.388(8)	58053.404 (Pickering and Zilio, 2001)
$4d^{10}\,6f_{\frac{5}{2}}$	58041.987(5)	58045.481 (Civiš et al., 2010)
$4d^{10}\,6f_{\frac{7}{2}}$	58042.063(4)	This work
$4d^{10}\,5g$	56711.565(3)	56711.1 (Shenstone, 1940)
$4d^{10}\,7d_{\frac{5}{2}}$	56705.467(2)	56705.498 (Pickering and Zilio, 2001), 56705.435 (Civiš et al., 2010)
$4d^{10}\,7d_{\frac{3}{2}}$	56699.832(3)	56699.768 (Pickering and Zilio, 2001), 56699.911 (Civiš et al., 2010)
$4d^{10}\,5f_{\frac{7}{2}}$	56691.397(2)	56691.4 (Shenstone, 1940), 56691.397 (Civiš et al., 2010)
$4d^{10}\,5f_{\frac{5}{2}}$	56691.275(2)	56691.4 (Shenstone, 1940), 56691.275 (Civiš et al., 2010)
$4d^{10}\,8p_{\frac{3}{2}}$	56660.597(3)	56660.559 (Pickering and Zilio, 2001), 56660.556 (Civiš et al., 2010)
$4d^{10}\,4f_{\frac{7}{2}}$	54204.745(3)	54204.73 (Shenstone, 1940)
$4d^{10}\,4f_{\frac{5}{2}}$	54204.729(2)	54204.73 (Shenstone, 1940)
$4d^{10}\,7p_{\frac{3}{2}}$	54121.108(1)	54121.129 (Pickering and Zilio, 2001), 54121.059 (Civiš et al., 2010)
$4d^{10}\,7p_{\frac{1}{2}}$	54041.037(2)	54040.99 (Brown and Ginter, 1977), 54041.087 (Civiš et al., 2010)
$4d^{10}\,7s_{\frac{1}{2}}$	51886.965(1)	51886.971 (Pickering and Zilio, 2001), 51886.954 (Civiš et al., 2010)
$4d^{10}\,6p_{\frac{3}{2}}$	48500.810(1)	48500.805 (Pickering and Zilio, 2001), 48500.804 (Civiš et al., 2010)
$4d^{10}\,6p_{\frac{1}{2}}$	48297.406(1)	48297.402 (Pickering and Zilio, 2001; Civiš et al., 2010)
$4d^{10}\,6s_{\frac{1}{2}}$	42556.147(1)	42556.152 (Pickering and Zilio, 2001)

detector's sensitivity. The present values of $7g_{\frac{7}{2},\frac{9}{2}}$ also differ from the values reported previously (Civiš et al., 2011): by 0.475 and 1.237 cm^{-1} respectively. We consider the present values to be the recommended ones, since in their extraction far more intensive (4646.928 and 4649.903 cm^{-1}) lines were involved as compared to the weak (2163.89 and 2171.118) lines used for extracting $7g_{\frac{7}{2},\frac{9}{2}}$ in the previous work (Civiš et al., 2011). The present values display fine-structure splitting of about 0.4 cm^{-1} which is more realistic than the 1.18 cm^{-1}-splitting resulting from the previous data (Civiš et al., 2011).

4. Conclusion

The present paper continues our studies of the IR emission spectra of metals in laser-induced plasma using Fourier-transform spectroscopy. Our measurements of Au, Ag

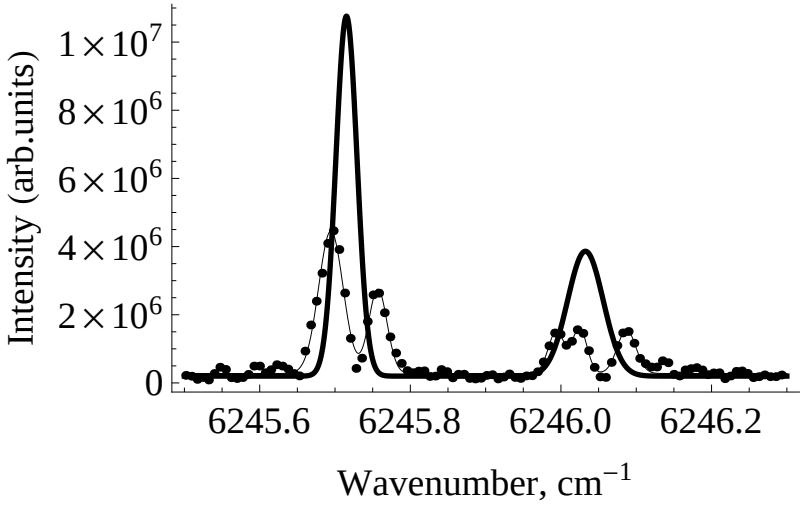

Figure 3. The $5s_{\frac{1}{2}}$–$5p_{\frac{1}{2},\frac{3}{2}}$ doublet lines of Cu I. The hyperfine components are fitted to Gaussian shape (thin curve), the parameters of the averaged lines (thick curves) are calculated using Equations 1.

and Cu spectra in four ranges (1200–1600, 1900–3600, 4100–5000 and 5200–7500 cm^{-1}) result in the reporting of 64 lines (32 for Au, 12 for Ag and 20 for Cu) not reported previously and in the refinement of 19 lines already published (9 for Au, 6 for Ag and 4 for Cu). We also provide a new classification for 4 Au lines and 1 Ag line.

The majority of the lines are due to transitions between the $N\mathrm{d}^{10}nl_j$ states with closed core ($N = 3, 4, 5$ for Cu, Ag and Au correspondingly) and $n = 4..10$. The line classification is performed using relative line strengths expressed in terms of transition dipole matrix elements calculated with the help of the Fues model potential. We show the results for the transition probabilities and oscillator strengths for transitions between the reported $5\mathrm{d}^{10}\,nl_j$ states of Au I (the previous papers contained such results for Ag (Civiš et al., 2010) and Cu (Civiš et al., 2011)).

For the classification of the observed IR lines, an important role is played by the f-, g- and h-states including those discovered in the present measurements. For all three elements considered, the most intensive emission line in 1200–1600 cm^{-1} corresponds to the 5g–6h transition (for an example, see the transition probability table 3 for Au). Indeed, due to small quantum defects (of the order of 10^{-2} and 10^{-3} for theg and h states respectively) this transition yields emission lines with close wavenumbers (1345–1347 cm^{-1}) for Au, Ag and Cu (see Figure 1).

The most prominent lines in the 1900–3600 cm^{-1} range are the pairs $n\mathrm{f}_{\frac{5}{2}}$–$5\mathrm{g}_{\frac{7}{2}}$ and $n\mathrm{f}_{\frac{7}{2}}$–$5\mathrm{g}_{\frac{9}{2}}$ where n is the principal quantum number of the first valence f-state; $n = 5$ for Au and $n = 4$ for Ag and Cu. For Au and Cu this nf–5g doublet occurs at 2517–2522 cm^{-1}(see Table 2 and the previous paper (Civiš et al., 2011)). Due to very small fine splitting of 4f state ($E\left(4\mathrm{f}_{\frac{7}{2}}\right) - E\left(4\mathrm{f}_{\frac{7}{2}}\right) = 0.016$ cm^{-1} in Ag (see Table 7) we saw only one Ag 4f–5g line (Civiš et al., 2010) at 2506 cm^{-1}.

In the 4100–5000 cm^{-1} range the most prominent emission takes place from the

Table 8. Cu I lines and their identification. Each of the four spectral ranges, 1200–1600, 1900–3600 cm^{-1} (only 2153 cm^{-1} line), 4100–5000 and 5200–7500 cm^{-1}, has its own scale of arbitrary units for the emission intensity.

Wavenumber (cm^{-1})	Intensity (arb. units)	SNR	FWHM (cm^{-1})	Identification
1277.179(5)	6.48×10^3	13.6	0.047(22)	$7s_{\frac{1}{2}}$–$7p_{\frac{3}{2}}$
1301.977(8)	6.09×10^3	9.69	0.073(28)	$7p_{\frac{3}{2}}$–$7d_{\frac{5}{2}}$
1344.291(3)	1.18×10^5	37.1	0.088(09)	5g –6h
1354.361(5)	2.76×10^4	12.2	0.087(15)	$5f_{\frac{7}{2}}$–$6g_{\frac{9}{2}}$
1361.593(5)	1.93×10^4	11.4	0.089(16)	$5f_{\frac{5}{2}}$–$6g_{\frac{7}{2}}$
1364.339(6)	1.46×10^4	11.6	0.083(18)	$6d_{\frac{5}{2}}$–$6f_{\frac{7}{2}}$
1366.874(6)	8.57×10^3	10.3	0.065(22)	$6d_{\frac{3}{2}}$–$6f_{\frac{5}{2}}$
2153.234(9)	6.20×10^4	8.51	0.099(29)	5g –7h
4221.555(6)	4.81×10^4	10.4	0.090(22)	$6p_{\frac{1}{2}}$–$7d_{\frac{3}{2}}$
4466.497(5)	8.69×10^4	9.44	0.108(18)	$6p_{\frac{3}{2}}$–$7d_{\frac{5}{2}}$
4646.928(5)	1.20×10^4	14.5	0.109(16)	$4f_{\frac{5}{2}}$–$7g_{\frac{7}{2}}$
4649.903(4)	1.15×10^5	16.9	0.122(12)	$4f_{\frac{7}{2}}$–$7g_{\frac{9}{2}}$
4680.179(3)	1.06×10^5	27.2	0.110(10)	$5d_{\frac{5}{2}}$–$7f_{\frac{7}{2}}$
4683.967(5)	6.93×10^4	17.8	0.105(14)	$5d_{\frac{3}{2}}$–$7f_{\frac{5}{2}}$
4842.019(8)	2.60×10^4	10.5	0.112(24)	$4d_{\frac{5}{2}}$–$6p_{\frac{3}{2}}$
4848.850(11)	6.13×10^3	3.59	0.054(51)	$4d_{\frac{3}{2}}$–$6p_{\frac{3}{2}}$
5484.3040(2)	1.06×10^7	267.	0.0349(5)	$4d_{\frac{5}{2}}$–$4f_{\frac{7}{2}}$
5487.269(2)	4.95×10^5	15.7	0.029(5)	$4d_{\frac{5}{2}}$–$4f_{\frac{5}{2}}$
5494.1249(2)	7.44×10^5	181.	0.0354(5)	$4d_{\frac{3}{2}}$–$4f_{\frac{5}{2}}$
6004.403(2)	1.31×10^5	25.8	0.047(7)	$5p_{\frac{1}{2}}$–$5d_{\frac{3}{2}}$
6004.721(3)	1.97×10^4	8.52	0.019(7)	$5p_{\frac{3}{2}}$–$5d_{\frac{3}{2}}$
6008.3527(6)	2.68×10^5	67.1	0.038(2)	$5p_{\frac{3}{2}}$–$5d_{\frac{5}{2}}$
6245.715(1)	3.71×10^5	18.1	0.033(4)	$5s_{\frac{1}{2}}$–$5p_{\frac{1}{2}}$
6246.033(2)	2.17×10^5	6.94	0.056(21)	$5s_{\frac{1}{2}}$–$5p_{\frac{3}{2}}$

7g-state to the first valence nf-state. The strongest lines in the 5200–7500 cm^{-1} are due to the n'd–nf transitions from first valence nf-states (with n values given above) and the first valence n'd-states ($n' = 6, 5, 4$ for Au, Ag and Cu correspondingly).

From the recorded spectra we extract revised values for the energies of 70 known levels (23 for Au, 20 for Ag and 27 for Cu) and of 15 previously not reported f-, g- and h-levels (8 for Au, 3 for Ag and 4 for Cu).

Acknowledgments

This work was financially supported by the Grant Agency of the Academy of Sciences of the Czech Republic (Grant No. IAA400400705).

Table 9. Revised values of some levels of Cu I

Term	Energy (cm^{-1})	Other sources
$3d^{10}\,7g_{\frac{7}{2}}$	60076.634(25)	60076.159 (Civiš et al., 2011)
$3d^{10}\,7g_{\frac{9}{2}}$	60076.217(19)	60074.980 (Civiš et al., 2011)
$3d^{10}\,7f_{\frac{5}{2}}$	60071.634(11)	This work
$3d^{10}\,7f_{\frac{7}{2}}$	60071.199(9)	60071.510 (Civiš et al., 2011)
$3d^{10}\,6h$	59268.422(20)	This work
$3d^{10}\,6g_{\frac{7}{2}}$	59266.776(10)	59267.202 (Civiš et al., 2011)
$3d^{10}\,6g_{\frac{9}{2}}$	59266.026(10)	59266.676 (Civiš et al., 2011)
$3d^{10}\,6f_{\frac{7}{2}}$	59259.436(30)	This work
$3d^{10}\,6f_{\frac{5}{2}}$	59259.916(28)	This work
$3d^{10}\,7d_{\frac{5}{2}}$	59250.565(27)	59250.72 (Shenstone, 1948)
$3d^{10}\,7d_{\frac{3}{2}}$	59249.303(26)	59249.46 (Shenstone, 1948)
$3d^{10}\,7p_{\frac{3}{2}}$	57948.572(11)	57948.57 (Ralchenko et al., 2008), 57948.71 (Shenstone, 1948)
$3d^{10}\,5g_{\frac{7}{2}}$	57924.549(26)	57924.610 (Civiš et al., 2011)
$3d^{10}\,5g_{\frac{9}{2}}$	57924.132(20)	57924.075 (Civiš et al., 2011)
$3d^{10}\,5f_{\frac{7}{2}}$	57911.591(10)	57908.7 (Shenstone, 1948), 57911.090 (Civiš et al., 2011)
$3d^{10}\,5f_{\frac{5}{2}}$	57905.120(10)	57905.2 (Shenstone, 1948), 57905.23 (Longmire et al., 1980), 57905.041 (Civiš et al., 2011)
$3d^{10}\,6d_{\frac{5}{2}}$	57895.097(29)	57895.1 (Shenstone, 1948), 57895.084 (Civiš et al., 2011)
$3d^{10}\,6d_{\frac{3}{2}}$	57893.042(27)	57893.05 (Shenstone, 1948), 57893.028 (Civiš et al., 2011)
$3d^{10}\,7s_{\frac{1}{2}}$	56671.387(10)	56671.387 (Shenstone, 1948)
$3d^{10}\,4f_{\frac{5}{2}}$	55429.739(26)	55429.8 (Shenstone, 1948)
$3d^{10}\,4f_{\frac{7}{2}}$	55426.357(20)	55426.3 (Shenstone, 1948)
$3d^{10}\,5d_{\frac{5}{2}}$	55391.004(9)	55391.292 (Shenstone, 1948), 55390.569 (Civiš et al., 2011)
$3d^{10}\,5d_{\frac{3}{2}}$	55387.667(10)	55387.668 (Shenstone, 1948), 55387.621 (Civiš et al., 2011)
$3d^{10}\,6p_{\frac{1}{2}}$	55027.748(26)	55027.74 (Shenstone, 1948), 55027.713 (Longmire et al., 1980), 55027.763 (Civiš et al., 2011)
$3d^{10}\,6p_{\frac{3}{2}}$	54784.074(35)	54784.06 (Shenstone, 1948), 54784.073 (Longmire et al., 1980), 54784.081 (Civiš et al., 2011)
$3d^{10}\,6s_{\frac{1}{2}}$	52848.735(9)	52848.749 (Shenstone, 1948), 52848.752 (Civiš et al., 2011)
$3d^{10}\,4d_{\frac{5}{2}}$	49942.057(20)	49942.057 (Shenstone, 1948)
$3d^{10}\,4d_{\frac{3}{2}}$	49935.614(26)	49935.2 (Shenstone, 1948)
$3d^{10}\,5p_{\frac{1}{2}}$	49383.168(19)	49383.26 (Shenstone, 1948)
$3d^{10}\,5p_{\frac{1}{2}}$	49382.818(10)	49382.95 (Shenstone, 1948)
$3d^{10}\,5s_{\frac{1}{2}}$	43147.22(1)	43137.209 (Shenstone, 1948)

References

Brown C M and Ginter M L 1977 *J. Opt. Soc. Am.* **67**(10), 1323–1327.

Brown C M and Ginter M L 1978 *J. Opt. Soc. Am.* **68**(2), 243–246.

Civiš S, Matulková I, Cihelka J, Kawaguchi K, Chernov V E and Buslov E Y 2010 *Phys. Rev. A* **81**(1), 012510.

Civiš S, Matulková I, Cihelka J, Kubelík P, Kawaguchi K and Chernov V E 2010 *Phys. Rev. A* **82**(2), 022502.

Civiš S, Matulková I, Cihelka J, Kubelík P, Kawaguchi K and Chernov V E 2011 *J. Phys. B* **44**(2), 025002.

Ehrhardt J C and Davis S P 1971 *J. Opt. Soc. Am.* **61**(10), 1342–1349.

Fano U 1974 *J. Phys. B* **7**(14), L401–L404.

George S, Grays A and Engleman, Jr. R 1988 *J. Opt. Soc. Am. B* **5**(7), 1500–1502.

Hanni M E, Keele J A, Lundeen S R and Sturrus W G 2008 *Phys. Rev. A* **78**(6), 062510.

Jannitti E, Cantù A M, Grisendi T, Pettini M and Tozzi G P 1979 *Phys. Scr.* **20**(2), 156–162.

Kawaguchi K, Sanechika N, Nishimura Y, Fujimori R, Oka T N, Hirahara Y, Jaman A and Civiš S 2008 *Chem. Phys. Lett.* **463**(1–3), 38–41.

Keele J A, Woods S L, Hanni M E, Lundeen S R and Sturrus W G 2010 *Phys. Rev. A* **81**(2), 022506.

Longmire M S, Brown C M and Ginter M L 1980 *J. Opt. Soc. Am.* **70**(4), 423–429.

Lundeen S R 2005 *in* P. R Berman and C. C Lin, eds, 'Advances In Atomic, Molecular, and Optical Physics' Vol. 52 of *Advances In Atomic, Molecular, and Optical Physics* Academic Press 525 B STREET, SUITE 1900, SAN DIEGO, CA 92101-4495 USA pp. 161 – 208.

MacAdam K B, Dyubko S F, Efremov V A, Gerasimov V G and Kutsenko A S 2009 *J. Phys. B* **42**, 165009.

Napier S A, Cvejanović D, Williams J F and Pravica L 2008 *Phys. Rev. A* **78**(3), 032706.

Pickering J C and Zilio V 2001 *Eur. Phys. J. D* **13**(2), 181–185.

Platt J R and Sawyer R A 1941 *Phys. Rev.* **60**(12), 866–876.

Ralchenko Y, Kramida A, Reader J and NIST ASD Team 2008 'NIST atomic spectra database (version 3.1.5)'.

Randall H M 1911 *Astrophys. J.* **34**, 1–20.

Shenstone A G 1940 *Phys. Rev.* **57**(10), 894–898.

Shenstone A G 1948 *Philos. Trans. R. Soc. London, Ser. A* **241**(832), 297–322.

Themelis S I 2010 *Phys. Rev. A* **81**(6), 064504.